Multimode-Photochromism Based on Strongly Coupled Dihydroazulene and Diarylethene

Thomas Mrozek,[a] Helmut Görner,*[b] and Jörg Daub*[a]

Abstract: Synthesis and photophysical/photochemical investigations of 1,8a-dihydro-2,3-bis(2,5-dimethy-3-thienyl)-azulene-1,1-dicarbonitrile (**1A**) and 1,8a-dihydro-2,3-diphenylazulene-1,1-dicarbonitrile (**2A**) are reported. The photoprocesses and thermal reactions of systems **1** and **2** were studied by time-resolved and steady-state techniques under various conditions. The dihydroazulene (DHA) – dithienylethene (DTE) conjugate **1A** is photochemically converted into the dihydrothienobenzothiophene (DHB) isomer **1C** and the vinylheptafulvene (VHF) isomer **1B**. System **2** exhibits exclusively DHA/VHF photochromism. For both systems the VHF form thermally reverts back into the DHA form. Their rate constant ($k_{B\rightarrow A}$) increases with the solvent polarity and the relaxation kinetics proceed by means of an activation barrier of 65 – 80 kJ mol^{-1}; $k_{B\rightarrow A}$ and the activation parameters of the isomerisation reactions are rather similar. The photostationary state of the **1A** → **1B** and **1A** → **1C** photoisomerisation is sensitive to the irradiation wavelength. The concept of cycloswitching is discussed.

Keywords: cycloswitching · diarylethenes · dihydroazulenes · electron transfer · photochromism

Introduction

Photochromism is an important tool in molecular switching and stands for the reversible interconversion between two entities (subunits) P_1 and P_2, whereby at least one reaction pathway has to be photochemical.[1] Interest in photochromism has received increased attention owing to potential application in energy and information processing at the molecular level[2, 3] as well as its involvement in biological processes such as colour vision.[4] Practical applications are also well established, as for example in optical transmission[5a] or in holography.[5b] Photochromism is also widely utilised from the molecular level up to complete devices, representative examples are: molecular switching of host/guest aggregates,[5c,d] of polymers,[6] of sol – gel thin films,[7] and pigment – protein complexes involved in proton pumping, vision or photomorphogenesis.[8] Organic chemistry has brought forth a number of photochromes many of which are involved in multimode or multifold switching. [9]

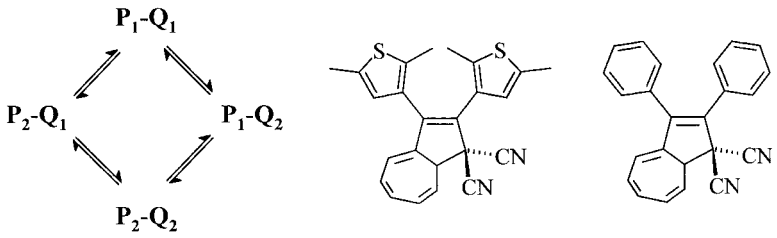

cyclic multistate switching | **DTE-DHA 1A** | **DPE-DHA 2A**

Scheme 1. Left: Graph indicating a cyclic four-state switching system. Compounds **1A** and **2A** as potential candidates for cyclic multistate switching.

Biphotochromic systems which are comprised of two photodynamic systems $P_1 \rightleftarrows P_2$ and $Q_1 \rightleftarrows Q_2$ are attractive candidates to continuously run cyclic multistate-switching since they may lead to four-step switching between the entities $P_1-Q_1/P_1-Q_2/P_2-Q_2/P_2-Q_1$ (Scheme 1). The thermal, photochemical and photophysical properties should be selectively controllable by substituents and by the electronic coupling of the two switching units.

This report deals with multistate switching of two covalently merged biphotochromic systems which differ in the mode of back and forward reactions: six-electron rearrangement versus ten-electron rearrangement and photochemical/photochemi-

[a] Prof. Dr. J. Daub, Dipl.-Chem. T. Mrozek
Institut für Organische Chemie der Universität Regensburg
Universitätsstrasse 31, 93053 Regensburg (Germany)
E-mail: joerg.daub@chemie.uni-regensburg.de

[b] Dr. H. Görner
Max-Planck-Institut für Strahlenchemie, 45413 Mülheim an der Ruhr (Germany)
E-mail: goerner@mpi-muelheim.mpg.de

0947-6539/01/0705-1028 $ 17.50+.50/0

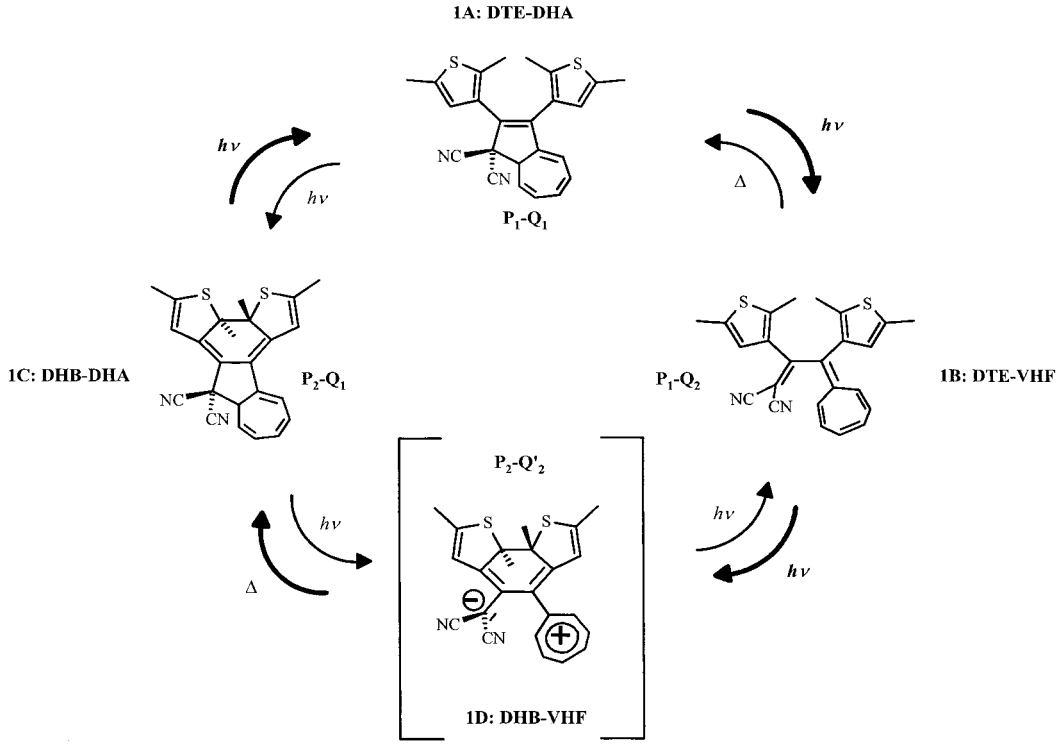

Scheme 2. Cyclic multistate switching of system **1**.

cal interconversion versus photochemical/thermal interconversion. Dihydroazulene (DHA)/vinylheptafulvene (VHF) photochromism,[10–15] that is, Q_1/Q_2 as a ten-electron rearrangement, is driven by a photochemical forward and a thermal back reaction. Dithienylethene (DTE)/dihydrothienobenzothiophene (DHB) photochromism,[16–20] that is P_1/P_2, is established by two photochemical reactions and represents a six-electron rearrangement. Since the two substructures in **1A** have one double bond in common they exemplify a strongly coupled system which with proper functionalisation may accomplish cyclic multistate-switching (Scheme 2). The syntheses, photochemical and photophysical properties of **1A** will be described. For comparison, 1,8a-dihydro-2,3-diphenylazulene-1,1-dicarbonitrile (**2A**) is included as a possible two-fold photochrome containing DHA/VHF, respectively diphenylethene (DPE)/dihydrophenanthrene (DHP) photochromism.

Abstract in German: *Die Synthese sowie die Ergebnisse der photophysikalischen und photochemischen Untersuchungen von 1,8a-Dihydro-2,3-bis(2,5-dimethyl-3-thienyl)azulen-1,1-dicarbonitril (**1A**) und 1,8a-Dihydro-2,3-diphenylazulen-1,1-dicarbonitril (**2A**) werden berichtet. Die photochemischen Prozesse und thermische Reaktionen von **1** und **2** wurden durch zeitaufgelöste und stationäre Methoden untersucht. Dihydroazulen (DHA)-Dithienylethen (DTE) **1A** lagert sich unter photochemischer Reaktionsführung in Dihydrothienobenzothiophen (DHB) (**1C**) und Vinylheptafulven (VHF) (**1B**) um. Verbindung **2** zeigt ausschliesslich die DHA/VHF Photochromie. Die VHF-Isomere beider Systeme werden jeweils thermisch in das entsprechende DHA-Isomer umgewandelt. Die diesbezügliche Geschwindigkeitskonstante ($k_{B\rightarrow A}$) erhöht sich mit steigender Lösungsmittelpolarität. Die Aktivierungsbarrieren betragen jeweils 65–80 kJ mol^{-1}. Der photostationäre Zustand der **1A**→**1B** beziehungsweise **1A**→**1C** Photoisomerisierung hängt von der Wellenlänge des eingestrahlten Lichtes ab. Das Konzept des „mehrstufigen und zyklischen Schaltens“ wird vorgestellt und diskutiert.*

Results

Steady-state photocolouration: The DTE/DHA isomer **1A** is colourless in all solvents used and has its main absorption at around 340 nm. Continuous irradiation, $\lambda_{irr} = 254$, 313 or 366 nm, or pulsed excitation, $\lambda_{exc} = 248$, 308 or 354 nm, of **1A** in acetonitrile yields spectra with two maxima, one at 360 nm, the other (λ_{col}) at 510 nm and a minimum around 420 nm (Figure 1a, Table 1).

The maximum ratio of absorbances at 360 nm (A^{I}_{360}) after excitation at 308 nm, and at 340 nm prior to irradiation (A^{0}_{340}) is $A^{I}_{360}/A^{0}_{340} = 1.5$. The spectral changes depend on solvents: On irradiation in ethanol the change of the absorption spectrum is similar to irradiation in acetonitrile, while in the case of the less polar toluene a small increase around 310 nm is observed, in addition to the above mentioned spectral changes (Figure 2a). This effect is more pronounced in methylcyclohexane (MCH) (Figure 3a or cyclohexane,[20] where the same two broad bands at 360 nm and around 500 nm were found for low conversion of **1A** upon irradiation at 254–366 nm. With higher conversion, however, a strong peak at 305 nm appears and the absorption in the visible range increases with its band blue-shifted. The ratio of absorbances at 305 nm after excitation at 308 nm, and at 340 nm prior to irradiation is $A^{I}_{305}/A^{0}_{340} \leq 1.4$. IR spectroscopy of **1A** in cyclohexane ($\tilde{\nu} = 2247$ cm^{-1}) shows the appearance of a C≡N absorption at lower wavenumber ($\tilde{\nu} = 2222$ cm^{-1}) upon

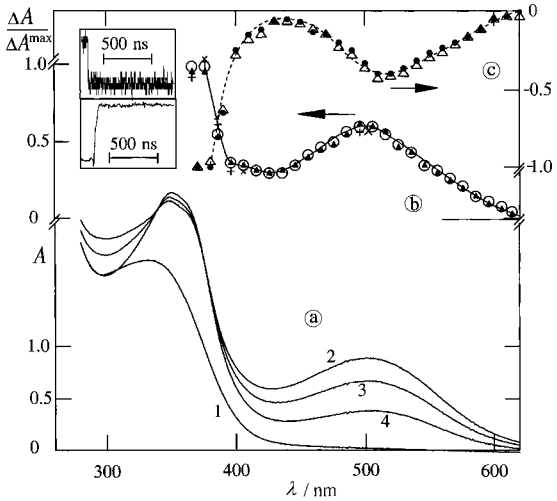

Figure 1. a) Absorption spectrum of **1A** in acetonitrile at 25 °C (1), after excitation at 308 nm (2) and after thermal relaxation (3,4); b) and c) transient absorption spectra at 50 ns (open) and 10 ms (full) after the pulse; b) using $\lambda_{exc} = 308$ nm (and signals after < 1 μs (+) and 1 ms (×) for $\lambda_{exc} = 248$ nm) and (c) $\lambda_{exc} = 530$ nm; insets: b) increase and c) decrease at 500 nm.

Table 1. Characteristic absorption maxima and quantum yields of isomerisation.[a]

System	Solvent	λ_B [nm]	λ_C [nm]	$\Phi_{A\rightarrow B}$[b]	$\Phi_{A\rightarrow C}$[c]
1	cyclohexane/MCH	305, 460	362, 500	0.15	0.12
	toluene	315, 480	360, 495	0.10	0.10
	acetonitrile	305, 500	360, 510	0.1	0.09
	ethanol	313, 510	360,512	0.1	0.08
2	cyclohexane/MCH	306, 455		0.30	
	toluene	313, 475		0.30	
	acetonitrile	315, 485		0.25	
	ethanol	316, 495		0.25	
3[d]	toluene	459		0.6	

[a] From light-induced changes of the absorption spectrum, $\lambda_{irr} = 366$ nm unless indicated otherwise. [b] Measured at λ_B (Vis). [c] Measured at λ_C (Vis). [d] Taken from ref. [12].

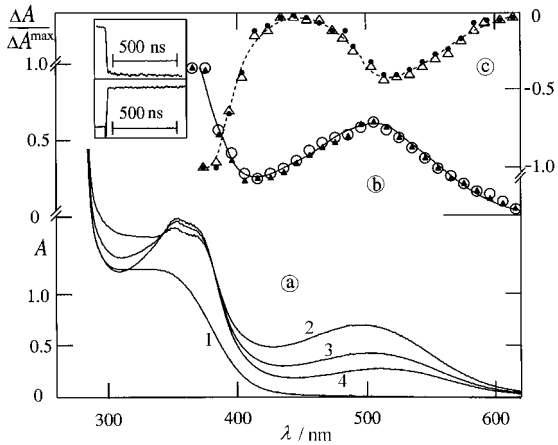

Figure 2. Spectra of **1A** in toluene; same conditions (except for $\lambda_{exc} = 248$ nm) as in Figure 1.

irradiation which subsequently disappears because of a thermal back reaction (**B** → **A**).

The absorption spectrum of **2A** ($\lambda_{max} = 340$ nm) after irradiation shows new maxima at 313 nm and $\lambda_{col} = 455$, 475 and 495 nm in MCH, toluene (Figure 4a and ethanol, respectively (Table 1). The ratio of absorbances at 313 nm after and at 340 nm prior to irradiation is $A^I_{313}/A^I_{340} \leq 1.8$ for $\lambda_{exc} =$ 308 nm. Two isosbestic points at 340–350 and 390–400 nm in various solvents, for example, at 344 and 400 nm in toluene, are indicative for only one photoproduct, intuitively the VHF form **2B** (otherwise a second product should have the same molar absorption coefficients at the two isosbestic points).

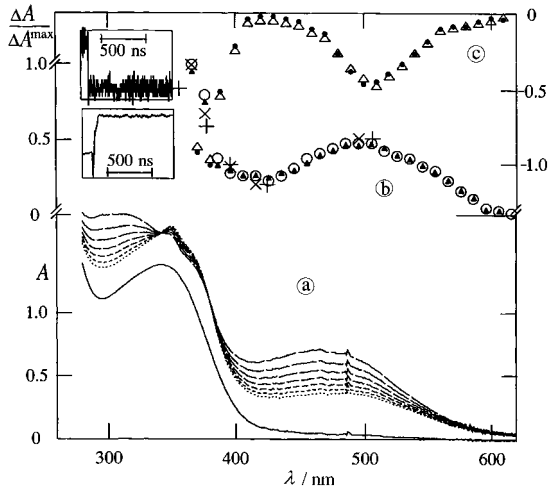

Figure 3. Spectra of **1A** in MCH, otherwise the same conditions as in Figure 1.

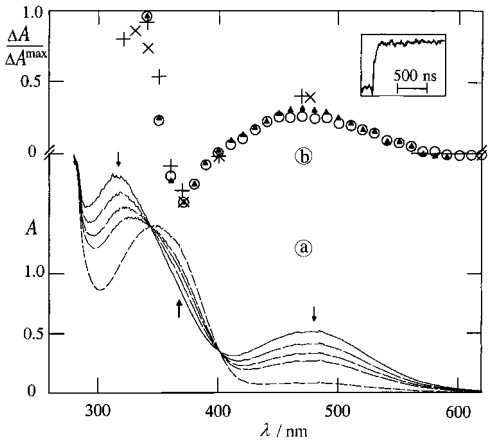

Figure 4. a) Absorption spectrum of **2A** in toluene at 25 °C after excitation at 308 nm (intervals of 10 s, 100 s for last spectrum); b) transient absorption spectra in MCH at 50 ns (open) and 10 ms (full) after the 308 nm pulse (and signals after < 1 μs (+) and 1 ms (×) for $\lambda_{exc} = 248$ nm).

As a rough measure of the process of photocolouration of **1A** and **2A**, the absorption at λ_{col} (A^I) can be used. A^I increases linearly with irradiation time (t_{irr}) with a curved dependence that approaches a maximum value in all solvents. The photoinduced A^I value for **1** partly reverts back when the light is removed (see below) and reaches a residual final value (A_e), $A_e = 0.3 - 0.5 \times A^I$. Repeated continuous irradiation at 366 nm (or pulsed excitation at 308 nm) and subsequent relaxation leads to virtually the same spectrum as that after

0947-6539/01/0705-1030 $ 17.50+.50/0 *Chem. Eur. J.* **2001**, *7*, No. 5

the initial procedure. In contrast to **1**, the A_e value of **2** is small throughout ($A_e < 0.02 \times A^I$).[20]

Time-resolved photocolouration: The transient absorption spectrum of **1A** ($\lambda_{exc} = 308$ or 354 nm) in several solvents at room temperature shows an increase within the laser pulse width (15–20 ns) or after disappearance of the fluorescence signal no further changes in the range of up to a few seconds. Examples with two maxima at < 380 nm and around λ_{col} in the visible range are shown in Figures 1b, 2b and 3b for **1** in acetonitrile, toluene and MCH, respectively. The presence and absence of oxygen has no observable effect throughout. Essentially the same two maxima and the minimum around 420 nm were monitored with $\lambda_{exc} = 248$ nm (Figures 1b and 3b).

The transient absorption spectrum of **2A** has also two maxima but also a bleaching range (Figure 4b). The bleaching at 400 nm (instead of a minimum in the case of **1**) is a consequence of the smaller molar absorption coefficient of photoproduct **2B** with respect to **2A**, and reflects changes in ground states. As a time-resolved measure of the yield of colouration the increase in absorbance (e.g. 1 μs after the 308 nm pulse) was used. The ΔA_{col} values of **2** are similar to those of **1** and depend only slightly on the solvent (Table 2).

Table 2. Absorption maxima and relative yield of photocolouration.[a]

Solvent	λ_{col}[b] [nm]		ΔA_{col}[c]	
	1	**2**	**1**	**2**
cyclohexane/MCH	470	455	0.9	1.0
CCl_4	490		0.8	
toluene	495	475	1.0	0.95
MTHF	500		0.8	
chloroform	500	480	0.8	0.9
dichloromethane	500		0.9	
DMF	500	485	0.9	0.8
acetonitrile	510	490	0.8	0.8
ethanol	515	495	0.8	0.8

[a] From light-induced changes of the absorption spectrum at 25 °C, λ_{exc} = 308 nm, unless indicated otherwise. [b] From the time-resolved increase. [c] Relative yield of the (Vis) maximum at < 1 μs; for **3** in toluene: $\Delta A_{col} = 8$.

Note that the ΔA_{col} value of 1,8a-dihydro-2-phenylazulene-1,1-dicarbonitrile (**3A**)[12] in toluene is eight times larger than that of **1**.

Thermal relaxation of the VHF (B) into the DHA (A) forms: Generally, the colouration of **1** and **2** in the visible range reverts back thermally. With the absorbance at time t (A_t), the initial photoinduced (A^I) and the final (A_e) values at λ_{col}, a first-order decay of $A'/A'^{max} = (A_t - A_e)/(A^I - A_e)$ was observed for **1** (inset of Figure 5). The rate constant (inverse relaxation time $k_{\mathbf{B}\rightarrow\mathbf{A}} = 1/\tau_{\mathbf{B}\rightarrow\mathbf{A}}$) depends on the solvent properties, the temperature and, to a minor extent, on the compound. At 25 °C $\tau_{\mathbf{B}\rightarrow\mathbf{A}}$ increases with decreasing solvent polarity (Table 3). It follows an Arrhenius dependence throughout. Semilogarithmic plots of the $1/\tau_{\mathbf{B}\rightarrow\mathbf{A}}$ values ($\mathbf{B} \rightarrow \mathbf{A}$ isomerisation) versus $1/T$ are shown in Figures 5 and 6 for system **1** and **2**, respectively. The activation energy (E_a) and pre-exponential factor are compiled in Table 3. For system **1** in cyclohexane or MCH the decay of A'/A'^{max}, when

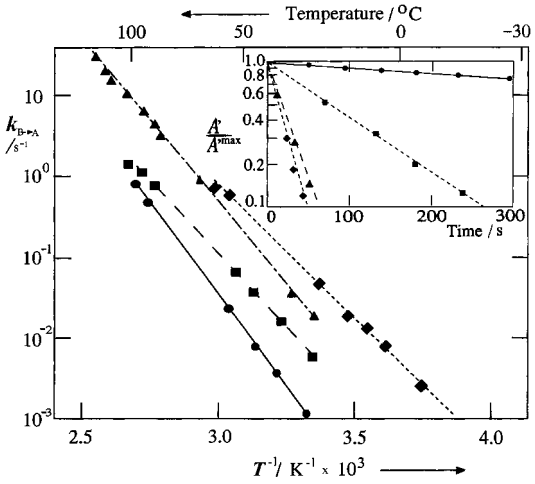

Figure 5. Rate constant of the relaxation kinetics (log scale) for system **1** in MCH (●), toluene (■), DMF (▲) and ethanol (◆) versus inverse temperature; $\lambda_{exc} = 308$ nm and $\lambda_{irr} = 366$ nm above and below approximately 50 °C, respectively; inset: plots of log $A'/A'^{max} = \log (A_t - A_e)/(A^I - A_e)$ versus time at 25 °C (same symbols).

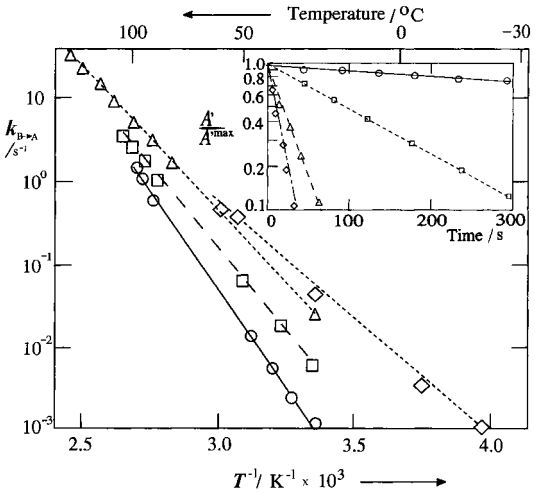

Figure 6. Rate constant of the relaxation kinetics (log scale) for system **2** in MCH (○), toluene (□), DMF (△) and ethanol (◇) versus $1/T$ (as in Figure 5).

registered at 300 nm, is also first-order ($\lambda_{irr} = 313$ or 366 nm). The same relaxation time at 300 nm and λ_{col} indicates that the intermediate photoproduct contains the VHF chromophore with maxima at 460 nm and 300 nm. In dimethylformamide (DMF) the highest temperature could be achieved, $E_a = 78\ kJ\,mol^{-1}$. E_a of system **1** is only slightly dependent on solvent properties and the significant effect of solvent polarity on the relaxation time at 25 °C is mainly owing to the same trends of both the pre-exponential factor A and E_a.

For system **2** in toluene the decay kinetics at 310 and 475 nm are identical (Figure 4a). This is also the case in a nonpolar solvent or in polar acetonitrile at room temperature, as well as in ethanol at lower temperatures, where $\tau_{\mathbf{B}\rightarrow\mathbf{A}}$ is long enough (up to 10^3 s). Moreover, the same $1/\tau_{\mathbf{B}\rightarrow\mathbf{A}}$ value was obtained from the increase in absorption within the two isosbestic points. The activation energy and the pre-exponential factor of system **2** are similar or slightly larger than those of system **1** (Table 3).

Table 3. Pre-exponential factor, activation energy and time for thermal relaxation.[a]

System	Solvent	A [$s^{-1} \times 10^{10}$]	E_a [kJ mol^{-1}]	$\tau_{B\rightarrow A}$ [s][b]
1B → **1A**	MCH	20	82	1100
	CCl_4			300
	toluene	1	70	130
	dichloromethane			50
	DMF	100	78	30
	acetonitrile	1	66	30
	ethanol	0.5	64	25
2B → **2A**	MCH	300	90	1200
	toluene	50	80	140
	DMF	100	78	30
	acetonitrile	1	66	20
	ethanol	3	68	18
3B → **3A**[c]	toluene	8	86	8×10^4
	ethanol	0.8	79	1×10^4

[a] Observed at 475 nm, using $\lambda_{exc} = 308$ nm and $\lambda_{irr} = 366$ nm above and below ca. 50 °C, respectively. [b] At 25 °C. [c] Taken from ref. [12].

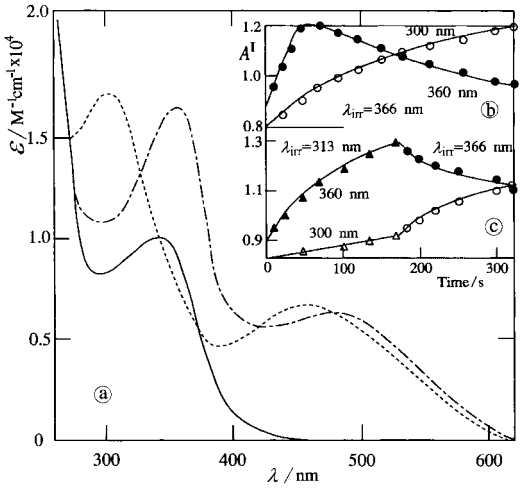

Figure 7. a) Absorption spectra of the **A**, **B** and **C** forms of **1** (full, dashed and dotted lines, respectively) and b), c) time dependences in MCH of A^{I}_{300} and A^{I}_{360} (open and full symbols, respectively) with $\lambda_{irr} = 366$ nm (circles) and $\lambda_{irr} = 313$ nm (triangles).

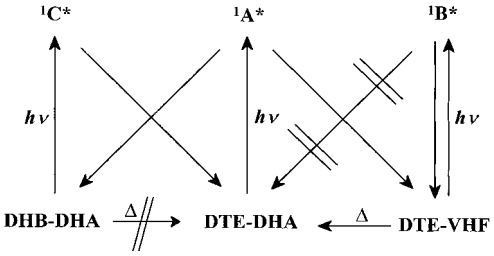

Scheme 3. Illustration of photochemical and thermal processes of system **1**.

Quantum yield of colouration: The two photoinduced colouration processes of **1** are a result of the ring opening at the DHA moiety (**A** → **B**) and the ring closure at the thienyl moiety (**A** → **C**) (Scheme 2). The former can be thermally reconverted but the latter can not.[20] In contrast, for **2** only one colouration process could be detected which is attributed to the ring opening at the DHA moiety. The light-induced colouration and subsequent thermal relaxation are similar to the respective processes in system **1**. The overall quantum yields of colouration of **1** and **2** in several solvents at ambient temperatures with $\lambda_{obs} = 460-500$ nm and $\lambda_{irr} = 366$ nm are rather similar. The quantum yield of ring opening ($\Phi_{A\rightarrow B}$) was found to be larger for system **2** than for system **1** (Table 1). Typical quantum yields of ring closure and ring opening reactions of diarylethenes are given in the literature.[17]

No marked effect of excitation wavelength, $\lambda_{irr} = 254$, 313 or 366 nm, on the overall spectral changes was found for **1** in solvents of medium and high polarity, where $\tau_{B\rightarrow A}$ is comparable with t_{irr}. The position of the photostationary state depends on the ε values of the three absorbing species and can therefore be shifted within certain limits by variation of λ_{irr}. In a nonpolar solvent the following spectral changes were found: For **1** in MCH with $\lambda_{irr} = 366$ nm the absorbance at 360 nm (A^{I}_{360}) strongly increases at first with t_{irr} and then decreases, while A^{I}_{300} becomes steadily larger (Figure 7b). With $\lambda_{irr} =$ 313 nm the slope for A^{I}_{300} is less steep and A^{I}_{360} becomes steadily larger. Switching then to $\lambda_{irr} = 366$ nm reverses the ratio A^{I}_{300}/A^{I}_{360} (Figure 7c). This indicates that the **C** band centred at 360 nm is stronger when converted back to **A** upon irradiation at 366 nm than at 313 nm, and that the **B** band (at 300 nm) acts as a sink for the absorbed light. Scheme 3 illustrates the photoprocesses of system **1**.

Photodecolouration: For **1** in several solvents at room temperature pre-irradiation (e.g. at 366 nm), thermal relaxation and subsequent irradiation at $\geq$436 nm leads to practically the same spectrum (of **1A**) as that prior to the initial colouration. The latter photodecolouration is due to the ring opening at the dihydrobenzene moiety, reaction **C** → **A**.[20] The quantum yield of decolouration (Φ_{-col}) in MCH was estimated to be 0.03. Φ_{-col} does not depend significantly on the solvent. No photodecolouration could be measured with system **2** owing to quantitative thermal **B** → **A** relaxation.

The time-resolved photodecolouration (**C** → **A**) was observed using $\lambda_{exc} = 530$ nm ($A_{530} = 0.2-0.6$). The transient absorption difference spectrum of system **1** in several solvents shows a decrease within the laser pulse width and no further changes in the range of up to a few seconds. Examples with two bleaching maxima at $<$380 nm and around $\lambda_{col} \approx 500$ nm and the minimum around 420 nm are shown in acetonitrile, toluene and MCH (Figures 1c, 2c and 3c, respectively). Oxygen has likewise no effect. For system **2** in several solvents no time-resolved spectral changes could be detected just after UV pre-irradiation ($A_{530} = 0.2-0.4$). This indicates that the yield of photoconversion of the DPE – VHF form **2B** is too low. A similar conclusion can also be drawn for system **3** since photodecolouration was found to be negligible, $\Phi_{-col} < 0.01$ in MCH or ethanol using $\lambda_{exc} = 530$ nm.

Triplet-state properties: At low temperatures, for example, in 2-methyltetrahydrofuran (MTHF) (Figure 8) or ethanol below -130 °C, a short-lived transient with maximum at 470 nm was observed for **1A**. This transient with a lifetime in the 2–10 μs range is assigned to the triplet state of **1A**. It is formed within the pulse width and has a similar spectrum to that under sensitised excitation at room temperature (see below).

0947-6539/01/0705-1032 $ 17.50+.50/0 *Chem. Eur. J.* **2001**, *7*, No. 5

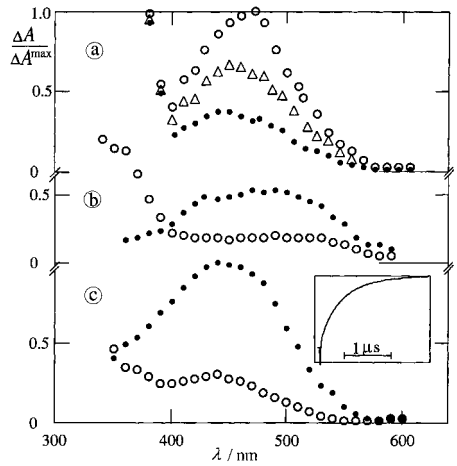

Figure 8. Transient absorption spectra of **1A** a) in MTHF at $-150\,^{\circ}C$ at <100 ns (○), 3 µs (△) and 10 µs (●) after the 308 nm pulse; b) and c) in acetonitrile at 25 °C at 30 ns (○) and 2 µs (●) after the 248 nm pulse, b) in the presence of acetophenone and c) of acetone; inset c): increase at 450 nm.

A short-lived transient (maximum at 470 nm, lifetime of a few µs) was also observed for **2A** in MCH, MTHF or ethanol between -130 and $-180\,^{\circ}C$. This transient is likewise assigned to the triplet state. It should be recalled that a similar transient in MTHF or ethanol below $-130\,^{\circ}C$ (maximum at 440 nm, lifetime of a few µs) has been assigned to the triplet state of the **A** form of **3**.[12]

When high-energy triplet donors (S) were applied to populate the triplet state of the **A** form of **1** (^{3}A*) in acetonitrile at room temperature, quenching of ^{3}S*, for example, with acetophenone (Figure 8b), and formation of a new transient was observed using $\lambda_{exc} = 248$ nm [Eq. (1)]. The new transient with a broad band centred around 480 nm should be assigned to state ^{3}A*.

$$^3S^* + \mathbf{A} \rightarrow S + {}^3A^* \quad (1)$$

Almost the same spectrum was recorded with acetone (Figure 8c), where the molar absorption coefficient of the ^{3}S* state is too low for detection at 320–350 nm. From linear plots of the rate constant of decay of ^{3}S* at their respective maxima, rate constants of quenching for acetophenone, xanthone and benzophenone were determined, the values are approximately $1 \times 10^{10}\,M^{-1}s^{-1}$. Naphthalene-sensitised excitation in ethanol with $\lambda_{exc} = 308$ nm leads to a comparable behaviour. The measurements are hampered by the requirements i) to excite **A** to only a minor extent and ii) to add a high enough concentration of **1A** to separate the spectra of the donor and acceptor triplets. Since the lifetime of the latter is only a few µs under our conditions, the results are a compromise and exclude further measurements with triplet donors of lower energy. Similar energy transfer effects were observed for **2A** in the presence of benzophenone (not shown). This new transient with a broad spectrum centred around 460 nm is also assigned to the ^{3}A* state of **2**.

Fluorescence: Weak fluorescence with a broad band centred at $\lambda_f = 470-480$ nm was observed for **1A** in several solvents at room temperature. The excitation spectrum is similar to the absorption spectrum. The quantum yield of fluorescence Φ_f is ≤ 0.003 (Table 4). At $-196\,^{\circ}C$ the emission and excitation spectra in MCH, MTHF or ethanol do not change significantly, whereas Φ_f is approximately 100-fold larger. Note that

Table 4. Wavelength of maximum and quantum yield of fluorescence.[a]

Compound	Solvent	λ_f [nm]	Φ_f
1A	MCH	480 (470)[b]	0.002 (0.2)
	toluene	480	0.003
	MTHF	470 (460)	0.003 (0.2)
	acetonitrile	470	0.001
	ethanol	480 (460)	0.002 (0.2)
2A	MCH	470 (470)	0.001 (0.3)
	MTHF	470 (460)	0.002 (0.2)
	ethanol	470 (465)	0.003 (0.2)
3A[c]	MTHF	460	<0.003 (0.9)

[a] At 25 °C using $\lambda_{exc} = 360$ nm. [b] Values in parentheses refer to $-196\,^{\circ}C$. [c] Taken from ref. [12].

Φ_f of **3A** at $-196\,^{\circ}C$ is even larger.[12] From a plot of $\log\Phi_f$ versus $1/T$ for **1A** in MTHF (not shown), an activation energy of 12 kJ mol^{-1} was obtained. No phosphorescence could be recorded in glassy media. This is in agreement with the rather short triplet lifetime (<10 µs). The fluorescence properties of **2A** (Table 4) are similar to those of **1A**.

Summary and Discussion

Photochromism of 1,8a-dihydro-2-phenyl-1,1-azulenedicarbonitrile (3A): The DHA/VHF photochromism of system **1** has features which are related to those of **3** (Scheme 4). The

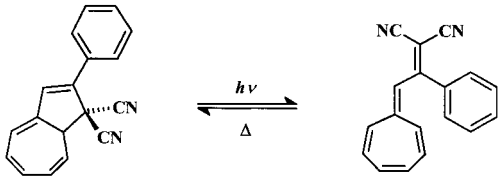

3A **3B**

Scheme 4. Photochromic system **3**.

photochemical and thermal properties of the DHA/VHF couple of **3** has been interpreted by the following reaction mechanism.[12] Irradiation populates the excited singlet state of the DHA form ($^1A^*$) and the ring opening takes place on the appropriate reaction coordinate in the excited singlet moiety since intersystem crossing is very small and can be neglected. A weakening of the (C-1–C-8a) bond is likely to be due to localisation of the negative charge at C-1 and the positive charge at a "tropenylium-type" substructure. This process is fast[21] and efficient and leads to the excited singlet state of the VHF form (^{1}B*) which is deactivated to the ground state by internal conversion. The quantum yield $\Phi_{\mathbf{A}\rightarrow\mathbf{B}}$ is 0.6 in toluene, where $\tau_{\mathbf{B}\rightarrow\mathbf{A}} = 8 \times 10^4$ s. The back conversion into the DHA form **3A** is rather slow and has to pass through

the s-*cis* VHF conformation of **3B**. A pathway from the ^{1}B* state into DHA can now be excluded. Φ_f for **3A** is $<10^{-2}$ at 25 °C and reaches almost unity at −196 °C. The small Φ_f value at low viscosities and higher temperatures results from the ring opening which competes successfully with fluorescence. In rigid glasses, however, the ring opening is completely suppressed since the viscosity in MCH, MTHF, or ethanol increases by approximately ten orders of magnitude. The slow ring opening below −130 °C opens up a weak pathway for the population of the triplet state of the DHA form of **3**.

Photochromism of 1,8a-dihydro-2,3-diphenylazulene-1,1-dicarbonitrile 2A: The results for the DHA/VHF couple of **2A** (Scheme 5) can, in principle, be interpreted on the basis of those for **3** where the VHF isomer is well characterised.[10–14] For **2** a pathway from the ^{1}B* state into DHA **2A** can be excluded, that is, ^{1}B* is deactivated by internal conversion at s-*cis* or s-*trans* geometry. The thermal relaxation kinetics proceed by the VHF → DHA activation barrier in the ground state. Both the energy of activation and the preexponential factor show marked dependencies on the solvent polarity (Table 3). Actually, two activation barriers along the s-*trans*-VHF → DHA ground state reaction pathway have to be considered. The larger one is assigned to s-*cis*-VHF → DHA transition (TS1), the lower one to s-*trans*-VHF → s-*cis*-VHF transition (TS2) (Scheme 6). This assumption is also supported by semiempirical quantum-mechanical calculations (PM3). According to the PM3 calculations, to reach the transition state TS2 which denotes the s-*trans*-/s-*cis*-VHF equilibrium requires by far less energy ($\sim$1 kJ mol^{-1}) than to reach TS1 ($>$100 kJ mol^{-1}) in the solvents used for simulation (Table 5).[22a,b] Moreover, the calculations show that the s-*cis*- and s-*trans*-conformations of the VHF have the same energy within the accuracy of the method.[22c] However, X-ray structural analysis from mono-substituted DHA/VHF derivatives show that the thermodynamically more stable s-*trans*-conformer is present in the crystalline state.[11b] Such vinylheptafulvenes are also assumed to dominate the s-*trans*-/s-*cis*-VHF equilibrium in solutions.[12, 14]

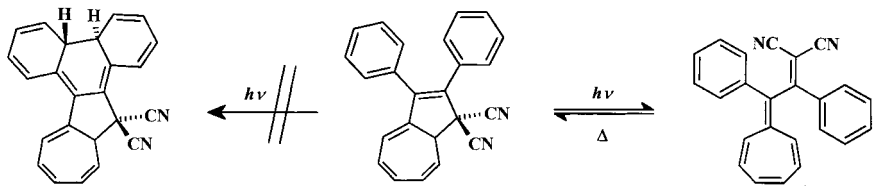

2C **2A** **2B**

Scheme 5. Photochromic system **2**.

For system **2** there could also be the possibility of a ring closure at the phenyl moiety[23] leading to the DHP – DHA form **2C**. However, this is not supported by the absorption spectra in nonpolar or polar solvents. They are identical either prior to irradiation or after the thermal VHF → DHA (**2B** → **2A**) relaxation. The UV-light-induced colouration of **2** is due only to formation of the VHF form. The solid line spectrum in Figure 4a can be simulated by using a conversion of approximately 60 % and molar absorption coefficients of $\varepsilon_{313} = 1.8 \times 10^4$, $\varepsilon_{400} = 0.2 \times 10^4$ and $\varepsilon_{475} = 0.5 \times 10^4$ M^{-1} cm^{-1} for **2B**.

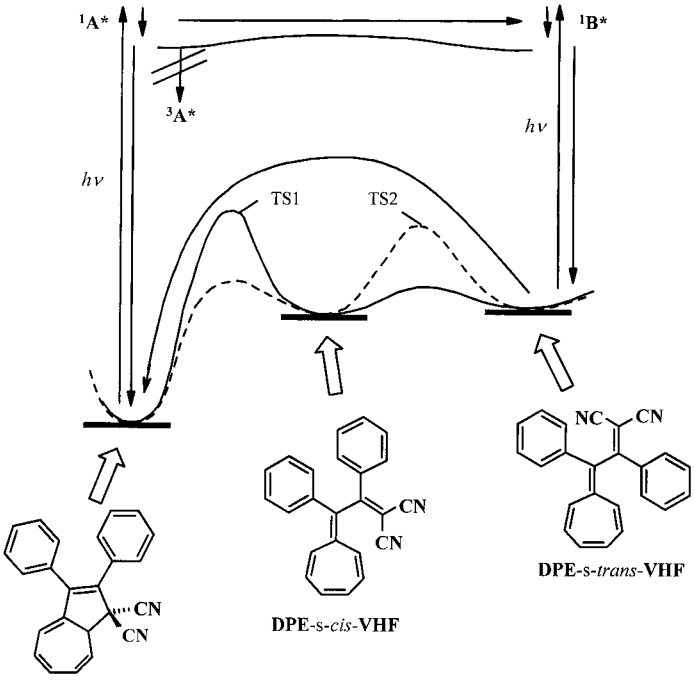

Scheme 6. Illustration of the reaction profiles of the photochromic system **2**.

The main differences between system **2** and **3** are that 1) the ratio of ε values in the UV absorption of the VHF versus the DHA forms of **2** is much larger and 2) the $\Phi_{A\rightarrow B}$ values of **2** are much smaller than those of **3** (Table 1). The faster thermal relaxation in polar solvents (Table 3), from a more polar transition state, has already been reported for other DHA/VHF systems (see also above).[14, 15]

Photochromism of 1,8a-dihydro-2,3-bis(2,5-dimethy-3-thi-

Table 5. Transition enthalpies ($\Delta\Delta H_f$ in kJ mol^{-1}) of system **2**.[a]

Solvent	DPE – DHA → TS1	DPE – s-*cis*-VHF → TS1	DPE – s-*cis*-VHF → TS2	DPE – s-*trans*-VHF → TS2
vacuum	215.05	168.57	4.48	0.63
cyclohexane	192.14	147.01	4.36	0.79
CH_2Cl_2	154.04	111.75	4.10	1.17
CH_3CN	142.57	101.62	4.10	0.84
CH_3OH	143.15	102.08	3.94	1.21

[a] Calculated values (PM3, COSMO) of system **2** regarding the DHA/VHF-reaction coordinate on the S_0-energy hypersurface. Transition states TS1, TS2 as indicated in Scheme 6.

0947-6539/01/0705-1034 $ 17.50+.50/0 *Chem. Eur. J.* **2001**, *7*, No. 5

enyl)azulene-1,1-dicarbonitrile (1A): The photocolouration of **1** is partly due to a photochemical ring opening, thereby forming the DTE–VHF form (**B**), and also due to a ring closure at the thienyl moiety leading to the DHB/DHA form (**C**). The thermally reversible ring closure, has been suggested to be related to the DHA/VHF photochromism (**A** ⇄ **B**), right side of Scheme 7. The thermally stable ring opening, is then

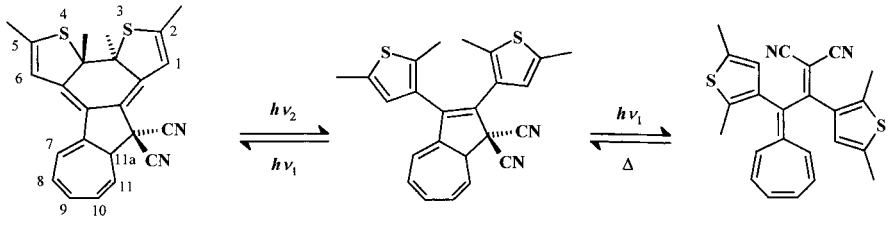

Scheme 7. Biphotochromic system **1**.

connected with the DTE/DHB photochromism (**A** ⇄ **C**), left side of Scheme 7.[20]

The absorption spectrum of **1C** in all solvents has two maxima at 360 nm and around 500 nm and two minima at approximately 300 and 420 nm, as revealed from the changes after irradiation (or repeated pulsing) at $\lambda_{irr} = 254-366$ nm and subsequent relaxation (Figures 1a–3a). The absorption spectrum of **1B** has one apparent maximum at 470–520 nm, as observed (within a short time interval $\tau_{B\rightarrow A}$) in solvents of medium and high polarity. This is also the case at a low conversion in nonpolar solvents, such as cyclohexane, where the relaxation is slowest (Table 3). In fact, λ_{col} of **1B** increases significantly with increasing solvent polarity, whereas λ_{col} of **1C** does not. At a higher conversion in MCH (Figure 3a), and to a smaller degree in toluene (Figure 2a), a further spectral change is observed between 280 and 400 nm. One possibility is that the VHF form of system **1** has no observable band in the UV range and an extra step is hypothesised from **1C** towards a new zwitterionic species (**1D** in Scheme 2) where the dihydroazulene ring is opened. This, however, can be excluded by analogy with system **3** and **2**. Additionally, IR spectroscopy of **1** in cyclohexane revealed a new photoinduced absorption band (C≡N vibration) located at lower energy with respect to the DHA-form **1A**, the formation of which is thermally reversible. This clearly demonstrates formation of the DTE/VHF species in agreement with the literature.[11b] This is also supported by ^{1}H NMR experiments after irradiation of **1A** at low temperature producing signals which disappear on thermal relaxation.[20] It is therefore suggested that **1B** has a second absorption maximum at 305–315 nm. This band may escape notice in solvents of larger polarity due to the relatively fast thermal relaxation at room temperature. Note that PM3 calculations (including solvent effects with and without consideration of configuration interaction) with the s-*trans*-VHF → DHA isomerisation (Scheme 8) give results with practically the same trends for the kinetic data ($\Delta\Delta H_f$) compared with the respective investigations concerning system **2** (see above). Therefore the right-hand part of Scheme 7 showing the thermal induced rearrangement is simplified as one transition state, which represents the ring-closure (TS1) of the azulene moiety, reaction s-*cis*-VHF → DHA (Scheme 8).

Thus, upon continuous irradiation of **1** as well as pulsed excitation below 400 nm, three species are present for absorption of the UV light, the DTE/DHA form **1A**, the DTE/VHF form **1B** and DHB/DHA form **1C** (Schemes 2 and 7). Eventually, a photostationary state is approached which is determined not only by the ε values at λ_{exc} and the $\Phi_{A\rightarrow B}$ and $\Phi_{A\rightarrow C}$ values, but also by t_{irr}, with respect to thermal relaxation $\tau_{B\rightarrow A}$. The complex behaviour is illustrated in Figures 7b and 7c with two different irradiation wavelengths for a case with long $\tau_{B\rightarrow A}$. The plots can be

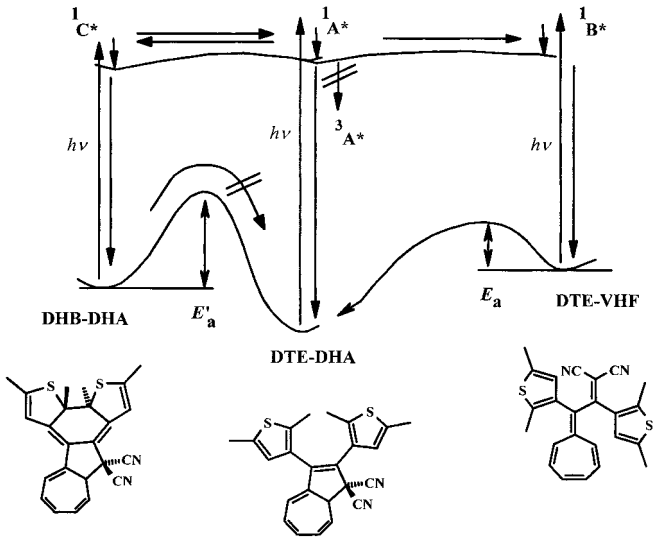

Scheme 8. Illustration of the reaction profiles of the biphotochromic system **1**.

analysed by using the spectra of **1B** and **1C** (Figure 7a). The maximum at 360 nm (Figure 7b) is the consequence of the efficiency of the **C** → **A** photoprocess which generates a maximum amount of **1C** within a short enough time. For **1** in MCH $\Phi_{A\rightarrow B}+\Phi_{A\rightarrow C}$ was found to be the same for $\lambda_{irr} = 313$ and 366 nm, that is Φ is independent of the irradiation wavelength. The data in Table 1 show that $\Phi_{A\rightarrow B}$ is comparable with $\Phi_{A\rightarrow C}$, which depends only slightly on the solvent polarity. On the other hand, because of the photochemical back reaction, the photostationary state favours **1B**.

The ^{1}H NMR spectrum of **1A** in [D$_8$]THF at −50 °C reveals a 2:1 mixture of two atropisomers. These have been attributed to two diastereomeric forms, both having pseudo-C_2 symmetry with respect to the two thiophenes and the chiral centre at the DHA moiety.[20] However, at room temperature a broadening of signals as a result of the fast equilibrium between those isomers was observed. No such effect could be detected for **2A**.

Mechanistic considerations: The suggested potential energy surfaces of **1** in the ground and excited singlet state along the two reaction coordinates for ring opening and ring closure are illustrated in Scheme 8. With respect to the ring opening they should be similar to those of **2** (Scheme 6).[24] Owing to the maxima around 500 nm for both **1C** and **1B**, the energy gap should be much smaller than that at the DTE/DHA geometry **1A**. In principle, the energy of the ^{1}B* state could be much lower than that of the ^{1}A* state. However, this cannot be the case for the ^{1}C* state, since both photoreactions (left side of Scheme 7, forth and back) occur. Therefore, the potential energy surfaces in the S_1 state are suggested to be rather flat. To account for the thermal stability of **1C** and the observed **B** → **A** back reaction, two barriers are postulated, the activation energy of the **C** → **A** step (E'_a) has to be significant larger than E_a.

The ring opening at the dihydroazulene moiety and the ring closure at the thienyl moiety at ambient temperatures compete since both Φ values are comparable (Table 1). They also successfully compete with other deactivation routes at the DTE–DHA geometry, such as fluorescence, internal conversion and intersystem crossing. The large increases of Φ_f with increased viscosities (Table 4) and the population of the observed triplet state indicates that these deactivation routes are enhanced at the expense of the two chemical reactions.

The photochemistry of system **2** is similar to that of **1**, apart from the ring closure at the arene moiety. The $\Phi_{A\rightarrow B}$ values are comparable (Table 1). Why is the DHA/DHP form **2C** not photochemically generated? One reason may be that the phenyl rings of **2A** are more twisted out of plane than the thienyl rings of **1A** (see below for X-ray structure of **2A**) and that the benzenoid energetics are unfavourable. The ring closure at the phenyl moiety can therefore not compete with ring opening toward **2B** and internal conversion at a geometry intermediate between **2A** and s-*trans* VHF/DPE. On the other hand, in glassy media, for example, in MCH, MTHF or ethanol below – 130 °C the ring opening is suppressed thereby enhancing the pathways for deactivation of **2** at the DHA geometry by means of fluorescence, internal conversion and intersystem crossing.

A few concluding remarks on cyclic multistate switching as depicted in Scheme 2 will be made. How can **D** be made photochemically accessible? Obviously, both the excited singlet and the ground state must be energetically more favourable than they are in **1**. In principle, this could be achieved by an electron-withdrawing substituent of the "dicyanovinyl bound" thienyl moiety which would stabilise the dicyanomethide group. The tropenylium substructure will already be stabilised by the sulfur of the dihydrothienobenzothiophene subunit.

An interesting point of Scheme 2 is the fact that the cyclic multistep process may occur in a clockwise or counterclockwise direction. Both sequences are gated by one thermal step each passing through two different pairs of constitutional isomers (**1D** → **1C** in the clockwise and **1B** → **1A** in the counter-clockwise process). Provided, the substitution pattern allows photochemical interconversions between the four biphotochromic structural isomers, cyclic versus noncyclic array-switching may be controlled by the thermal triggering step which also opens up either the clockwise or counterclockwise reaction pathway.

Experimental Section

General: Melting points were uncorrected and were measured on a Büchi SMP 20 and Reichert Thermovar. IR spectra were recorded with a Bio-Rad FT-IR Spectrometer FTS-155. EIMS (70 eV) were measured with a Varian CH-5. NMR spectra were recorded with either a Bruker AC250 (24 °C) or a ARX (400) (21 °C) spectrometer at 250/400 MHz for ^{1}H, respectively; room temperature, unless otherwise noted. Chemical shifts δ were recorded against TMS as internal standards (dpt = doublet of pseudo triplet). Solvents and reagents were used as purchased without further purification unless stated otherwise: $CHCl_3$ and CH_3CN were dried over P_2O_5. Benzene was dried with Na. The reaction progress was monitored by TLC.

Synthesis and molecular structure: Compounds **1A** and **2A** were synthesised using the "fulvene route"[11c, 15] (Scheme 9): Starting material for the synthesis of **1A** was 2,5-dimethylthiophen-3-ylacetic acid **4a**, which was converted into the acid chloride **5a** with $SOCl_2$ in chloroform. Compound

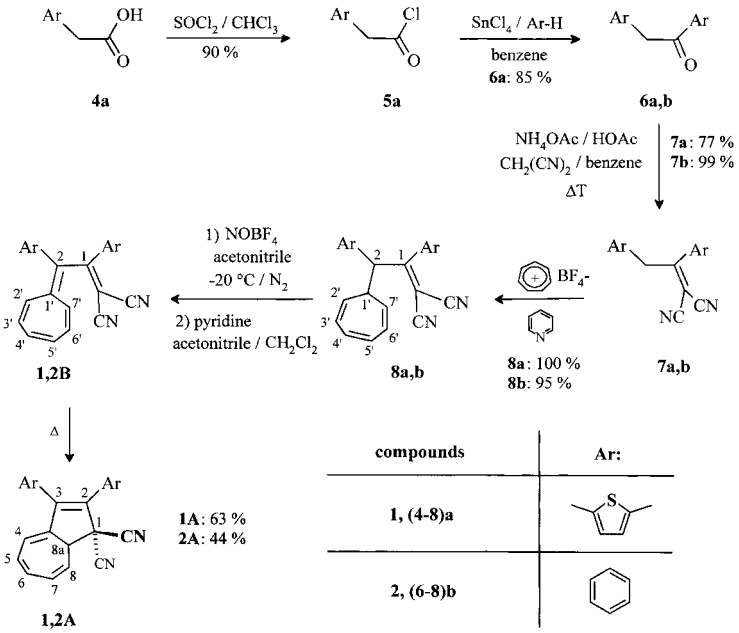

Scheme 9. Synthesis of **1A** and **2A**.

5a gave ketone **6a** by reaction with 2,5-dimethylthiophene and $SnCl_4$ in benzene by means of a Friedel–Crafts acylation. The ketones **6a** and **6b** were converted into the corresponding malonodinitrile derivatives **7a** and **7b** by Knoevenagel condensation (malonodinitrile, NH_4OAc/HOAc, in benzene), respectively. Tropylium tetrafluoroborate and **7a**, or **7b** led to **8a** or **8b**, respectively. In a final two-step process, dehydrogenation occurred in a one-pot reaction by hydride abstraction with $NOBF_4$ and subsequent deprotonation of the resulting tropylium ions with pyridine. At room temperature the primarily formed VHFs **1B** and **2B** immediately rearrange to the corresponding DHAs **1A** and **2A**, respectively.

X-ray crystal structure analysis of 2A: Single crystals were obtained by recrystallisation of **2A** from THF/*n*-hexane. Diffraction data were collected on a STOE/IPDS diffractometer ($Mo_{K\alpha}$ radiation, graphite monochromator) in the φ rotation scan mode at 173 K using an Oxford Cryosystem Cooler.[25a] The structure determination was achieved with direct methods by using SIR-97[25b] and refinements with full-matrix anisotropic least-squares on F^2 with SHELXL-97.[26a] The hydrogen atoms were located by difference fourier synthesis and refined isotropically. The graphic was performed with ORTEP.[26b] Refinement parameters and crystal data are

0947-6539/01/0705-1036 $ 17.50+.50/0 *Chem. Eur. J.* **2001**, *7*, No. 5

given in Tables 6 and 7.[27] The solid state structure of **2A** reveals the typical boat structure of the seven-membered ring and two slightly twisted phenyl groups ($\Theta \approx 52^\circ$) out of the plane of the five-membered ring minimising the sterical hindrance between the aryl groups (Figure 9).

Table 6. Structure determination summary of **2A**.

formula	$C_{24}H_{16}N_2$
M_W	332.39
T [K]	173 (1)
crystal system	triclinic
space group	$P\bar{1}$
a [Å]	9.2231 (10)
b [Å]	10.8547 (12)
c [Å]	19.0671 (12)
α [°]	97.583 (13)
β [°]	97.466 (13)
γ [°]	104.189 (13)
V [Å^3]	1808.1 (3)
Z	4
ρ_{calcd} [Mg m^{-3}]	1.221
μ [mm^{-1}]	0.07
F (000)	696
crystal size [mm]	0.42 × 0.40 × 0.14
colour	translucent, pale-green
scan range (Θ) [°]	1.96–25.68
index ranges	$-11 (h \le 11$ $-13 \le k \le 13$ $-22 \le l \le 23$
reflections collected/unique	13176/6387
R(int)	0.0625
data/restraints/parameters	6387/0/597
goodness-of-fit on F^2	0.870
final R indices [$I > 2\sigma(I)$] $R1$	0.0523
$wR2$	0.1175
R indices (all data) $R1$	0.0926
$wR2$	0.1328
largest diff. peak and hole [e Å^{-3}]	0.223/ − 0.228

Table 7. Selected structural features of **2A**[a].

	X-ray	AM1[b]	PM3[b]
bond lengths [Å]			
C1–C2	1.553	1.531	1.525
C2–C3	1.357	1.359	1.352
C3–C4	1.443	1.470	1.468
C4–C5	1.509	1.510	1.508
C5–C6	1.502	1.482	1.490
C6–C7	1.325	1.343	1.339
C7–C8	1.456	1.441	1.448
C8–C9	1.355	1.347	1.343
C9–C10	1.427	1.440	1.445
C10–C4	1.349	1.344	1.342
C1–C5	1.560	1.573	1.576
C1–C23	1.487	1.461	1.466
C1–C24	1.483	1.459	1.464
C23–N1	1.140	1.162	1.158
C24–N2	1.142	1.162	1.158
C2–C11	1.461	1.454	1.463
C3–C17	1.486	1.445	1.463
bond angles [°]			
C23-C1-C24	106.4	109.0	107.7
C1-C2-C3	109.0	111.1	111.4
C2-C3-C4	112.4	111.1	111.0
C3-C4-C5	109.0	108.7	109.0
C2-C1-C5	104.7	104.2	104.3
C1-C5-C4	103.9	104.8	104.3
C4-C5-C6	107.4	112.3	110.4
C5-C6-C7	120.7	123.9	123.1
C6-C7-C8	125.9	126.9	126.0
C7-C8-C9	124.7	126.5	125.8
C8-C9-C10	126.2	126.3	125.7
C4-C10-C9	124.4	125.6	124.4
C5-C4-C10	121.9	125.2	125.0
C1-C5-C6	117.4	115.7	116.1
C3-C4-C10	129.1	126.0	125.9
torsion angles [°]			
C1-C2-C11-C16	51.7	76.3	87.8
C2-C3-C17-C22	52.4	52.0	59.5

[a] Numbering as defined in X-ray structure analysis (Figure 9). [b] AM1-, PM3-optimised geometries in vacuum without using CI.

Tropylium tetrafluoroborate,[28] 2,5-dimethylthiophene-3-ylacetic acid (**4a**),[29] 2-phenyl-1,8a-dihydroazulene-1,1-dicarbonitrile (**3A**),[11b] 1,2-diphenylethylidene-propanedinitrile (**7b**)[30] have been prepared as previously reported.

2,5-Dimethylthiophene-3-yl-acetic acid chloride (5a): Under a N_2 atmosphere, $SOCl_2$ (8.1 mL, 0.11 mol) was rapidly added to a stirred solution of 2,5-dimethylthiophene-3-ylacetic acid (**4a**, 12.6 g, 74.0 mmol) in $CHCl_3$ (40 mL). Stirring was continued at room temperature as long as gas evolution proceeded (approximately 1 h). The solution was refluxed (60–70 °C) for an additional 2 h. Excess reagent and solvent were then removed under vacuum and the dark liquid residual was placed under reduced pressure to afford a greenish-brown liquid (13 g, 67 mmol, 90%). B.p. 84 °C at 0.7 mmHg; IR (film): $\tilde{\nu} = 2950, 2922, 2864, 2742, 1895, 1797, 1447, 1221, 1147, 1099, 1000, 952, 831, 781, 743, 690, 674, 610$ cm^{-1}; ^{1}H NMR (250 MHz, $CDCl_3$): $\delta = 2.33$ (br s, 3H, Me), 2.38–2.40 (m, 3H, Me), 3.97 (s, 2H, -CH_2-), 6.52 (q, $J = 1.1$ Hz, 1H, thiophene-H).

Bis(2,5-dimethylthiophene-3-yl)ethanone (6a): A solution of $SnCl_4$ (0.63 mL, 5.4 mmol) in dry benzene (5 mL) was added dropwise (≈15 min) to a solution of **5a** (1.0 g, 5.3 mmol) and 2,5-dimethylthiophene (0.62 mL, 5.4 mmol) in dry benzene (15 mL) in a dry flask immersed in ice. During the addition, the mixture turned deep red. After completion of the addition, the mixture was diluted with additional benzene (10 mL) and allowed to warm up to room temperature. The mixture was hydrolysed with HCl (2N, 20 mL), and the colour turned from red to green. The organic layer was separated and the water phase extracted four additional times with benzene. The combined organic phases were washed once with water and stirred over anhydrous Na_2SO_4. After filtration and evaporation of the solvent, column chromatography on silica gel using CH_2Cl_2/PE 2:1 afforded a red resin (1.2 g, 4.5 mmol, 85%). IR (KBr): $\tilde{\nu} = 2921, 2862, 1671, 1550, 1480, 1447, 1361, 1253, 1223, 1140, 975, 826, 777, 684, 635$ cm^{-1}; ^{1}H NMR (250 MHz, $CDCl_3$): $\delta = 2.31$ (br s, 3H, Me), 2.39 (qd, $J^1 = 1.1$ Hz, $J^2 =$

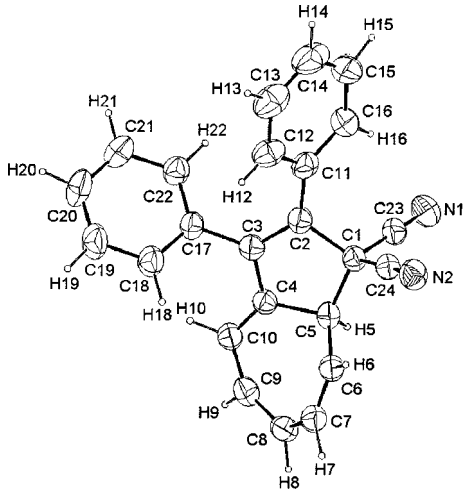

Figure 9. ORTEP-drawing of the molecular structure of *S*-**1A** with the atomic numbering scheme. Displacement ellipsoids are drawn at the 50% probability level.

0.6 Hz, 3H, Me), 2.42 (qd, $J^1 = 1.0$ Hz, $J^2 = 0.5$ Hz, 3H, Me), 2.69 (br s, 3H, Me), 3.91 (s, 2H, -CH_2-), 6.47 (q, $J = 1.0$ Hz, 1H, thiophene-H), 7.04 (q, $J =$ 1.2 Hz, 1H, thiophene-H); elemental analysis calcd (%) for $C_{14}H_{16}S_2$: C 63.60, H 6.10; found C 63.44, H 6.15; MS (70 eV, EI): *m/z* (%): 264 (19.68) $[M]^{\bullet+}$, 139 (100) $[M - 2,5\text{-dimethylthienyl}]^{\bullet+}$.

1,2-Bis(2,5-dimethylthiophene-3-yl)ethylidenepropanedinitrile (7a): In a flask, equipped with a reflux condenser, water separation funnel and an addition funnel, a mixture of **6a** (4.5 g, 17 mmol) and malonodinitrile (3.4 g, 51 mmol) dissolved in benzene (120 mL) was refluxed for 21 h, while a solution of HOAc (30 mL) and NH_4OAc (10 g) was added in portions through the additional funnnel to the reaction mixture (TLC control). The reaction mixture was diluted with benzene and water (100 mL each). After separation of the organic layer, the aqueous phase was extracted four times with benzene. The combined organic layers were washed once with water, dried over anhydrous Na_2SO_4 and filtered. After evaporation of the solvent by rotatory evaporator, column chromatography on silica and ethyl acetate/PE 1:10 afforded a red solid, which still contained some impurities. Recrystallisation from *n*-hexane/Et_2O/CH_2Cl_2 afforded colourless needles (4.0 g, 13 mmol, 77%). M.p. 91–92 °C; IR (KBr): $\tilde{\nu} = 2919$, 2859, 2230, 1575, 1494, 1442, 1265, 1211, 1147, 1098, 1033, 834, 806, 586, 493 cm^{-1}; ^1H NMR (250 MHz, $CDCl_3$): $\delta = 2.09$ (s, 3H, Me), 2.17 (s, 3H, Me), 2.32–2.34 (m, 3H, Me), 2.39–2.41 (m, 3H, Me), 3.89 (s, 2H, -CH_2-), 6.30–6.32 (m, 1H, thiophene-H), 6.44 (q, $J = 1.1$ Hz, 1H, thiophene-H); MS (70 eV, EI): *m/z* (%): 312.2 (100) $[M]^{\bullet+}$, 200 (54.85) $[M - 2,5\text{-dimethylthienyl}]^{\bullet+}$; elemental analysis calcd (%) for $C_{17}H_{16}S_2N_2$: C 65.35, H 5.16, N 8.97; found C 64.71, H 5.50, N 7.91.

2-(2′,4′,6′-Cycloheptatrien-1′-yl)-1,2-bis(2,5-dimethylthiophene-3-yl)-ethylidenepropanedinitrile (8a): A suspension of tropenylium tetrafluoroborate (0.82 g, 4.6 mmol) and **7a** (1.4 g, 4.5 mmol) in pyridine (10 mL) was stirred for 1 h (TLC control). The resulting yellow solution was diluted with Et_2O and HCl (2N, 50 mL each) and stirred for another 10 min. After separating the organic layer, the aqueous phase was extracted twice with Et_2O. The combined organic layers were washed once with HCl (2N, 20 mL) and water, respectively, dried over anhydrous Na_2SO_4 and filtered. After evaporation of the solvent by rotatory evaporation, column chromatography on silica gel using ethyl acetate/PE 1:10 afforded a yellow resin (1.8 g, 4.8 mmol, 100%) after drying in high vacuum ($< 10^{-4}$ mbar). IR (film): $\tilde{\nu} =$ 3022, 2923, 2864, 2233, 1572, 1446, 1217, 1146, 838, 802, 756, 724, 702, 669 cm^{-1}; ^1H NMR (400 MHz, [D_6]DMSO, 353.0 K): $\delta = 1.77$ (br s, 3H, Me), 2.22–2.23 (m, 3H, Me), 2.25–2.26 (m, 3H, Me), 2.32–2.33 (m, 3H, Me), 2.55–2.63 (m, 1H, 1′-H), 4.45 (d, $J = 12.1$ Hz, 1H, 2-H), 5.03–5.09 (m, 1H, 2′/7′-H), 5.45–5.51 (m, 1H, 2′/7′-H), 5.83 (br s, 1H, thiophene-H), 6.13–6.22 (m, 2H, 3′/6′-H, thiophene-H), 6.40–6.45 (m, 1H, 3′/6′-H), 6.66–6.72 (m, 1H, 4′/5′-H), 6.74–6.80 (m, 1H, 4′/5′-H); MS (70 eV, EI): *m/z* (%): 402 (0.31) $[M]^{\bullet+}$, 90.9 (100) $[C_7H_7]^{\bullet+}$; elemental analysis calcd (%) for $C_{24}H_{22}S_2N_2$: C 71.96, H 5.54, N 6.99; found C 71.51, H 5.71, N 7.39.

1,8a-Dihydro-2,3-bis(2,5-dimethylthiophene-3-yl)azulene-1,1-dicarbonitrile (1A): In a light-protected three-necked flask, a stirred solution of **8a** (0.78 g, 1.9 mmol) in dry acetonitrile (40 mL) was treated dropwise with $NOBF_4$ (0.44 g, 3.8 mmol) at −10 °C under N_2 bubbling. Stirring was continued for 45 min in total (TLC control). The yellow-brown solution was diluted with dry CH_2Cl_2 (100 mL), followed by dropwise addition of pyridine (0.32 mL, 4.0 mmol). The resulting dark-red mixture was stirred for another 15 min. The organic layer was separated, washed twice with water, and dried over anhydrous Na_2SO_4 and filtered. Afterwards, the solvent was evaporated with a rotatory evaporator, and the crude product was subjected to column chromatography on silica gel with CH_2Cl_2/PE 1:1 affording a greenish-yellow solid (0.48 g, 1.2 mmol, 63%) after drying in high vacuum ($< 10^{-4}$ mbar). M.p. 61–62.5 °C; IR (KBr): $\tilde{\nu} =$ 3023, 2954, 2922, 2860, 2248, 1741, 1441, 1145, 705, 493 cm^{-1}; ^1H NMR (400 MHz, [D_8]THF, 223.0 K, two atropisomers in the ratio 1:0.45): $\delta = 1.68$ (s, 3H, Me, isomer 1), 1.77 (s, 3H, Me, isomer 2), 1.80 (s, 3H, Me, isomer 1), 2.00 (s, 3H, Me, isomer 2), 2.34 (s, 3H, Me, isomer 2), 2.38 (s, 3H, Me, isomer 1), 2.45 (s, 3H, Me, isomer 2), 2.46 (s, 3H, Me, isomer 1), 3.63 (dpt, $J^1 = 4.4$ Hz, $J_{pt} =$ 1.7 Hz, 1H, 8a-H, isomer 1), 3.74–3.77 (m, 1H, 8a-H, isomer 2), 5.67 (dd, $J^1 = 9.7$ Hz, $J^2 = 4.4$ Hz, 1H, 8-H, isomer 1), 5.77 (dd, $J^1 = 10.0$ Hz, $J^2 =$ 4.1 Hz, 1H, 8-H, isomer 2), 6.12–6.18 (m, 2 × 1H, 2 × 4-H, isomers 1 and 2), 6.32–6.38 (m, 2 × 1H, 2 × 7-H, isomers 1 and 2), 6.40 (br s, 1H, thiophene-H, isomer 2), 6.50–6.68 (m, 5H, isomer 1: thiophene-H, 5-H, 6-H, isomer 2: 5-H, 6-H), 7.10–7.12 (m, 1H, thiophene-H, isomer 2), 7.14–7.16 (m, 1H, thiophene-H, isomer 1); MS (70 eV, EI): *m/z* (%): 400.4 (100) $[M]^{\bullet+}$; elemental analysis calcd (%) for $C_{24}H_{20}S_2N_2$: C 71.96, H 5.03, N 6.99; found C 70.97, H 5.54, N 6.27.

1,2-Bis(2,5-dimethylthiophene-3-yl)-2-(2′,4′,6′-cycloheptatriene-1′-ylidene)-ethylidenepropanedinitrile (1B): Compound **1B** was prepared by irradiation of solutions of **1A** in various solvents.

3a,3b,11A,12-Tetrahydro-2,5-dimethyl-*trans*-3a,3b-dimethylazuleno-[2′,3′:3″,4″]benzo[1″,2″-b‴:6″,5″-b⁗]dithiophene-12,12-dicarbonitrile (1C): Compound **1C** was prepared by irradiation of a quartz NMR tube containing a solution of **1A** in [D_8]THF (3.8 mM, $\lambda_{irr} = 254$ nm). Total irradiation time: 5 h with two breaks (2.5 h) after each 2.5 h of irradiation. ^1H NMR (400 MHz, [D_8]THF, 223.0 K, subtraction spectra): $\delta = 1.90$ (s, 3H, Me), 2.02 (s, 3H, Me), 2.21 (s, 3H, Me), 2.25 (d, $J = 1.2$ Hz, 3H, Me), 2.72 (dpt, $J^1 = 5.3$ Hz, $J_{pt} = 1.3$ Hz, 1H, 11a-H), 5.42 (dd, $J^1 = 9.3$ Hz, $J^2 =$ 5.3 Hz, 1H, 11-H), 6.34–6.41 (m, 2H, thiophene-H, 10-H), 6.53–6.55 (m, 1H, thiophene-H), 6.68–6.74 (m, 2H, 9-H, 7-H), 6.89 (dd, $J^1 = 11.2$ Hz, $J^2 = 6.3$ Hz, 1H, 8-H).

2-(2′,4′,6′-Cycloheptatrien-1′-yl)-1,2-diphenylethylidenepropanedinitrile (8b): Compound **8b** was prepared in an analogous manner to **8a** from **7b** (1.0 g, 4.1 mmol), tropenylium tetrafluoroborate (0.75 g, 4.2 mmol) and pyridine (10 mL) within a reaction time of 2 h. Chromatography on silica gel using AcOEt/PE 1:5 afforded a yellowish resin (1.3 g, 3.9 mmol, 95%). IR (KBr): $\tilde{\nu} =$ 3061, 3023, 2963, 2233, 1573, 1494, 1447, 1262, 1083, 1028, 811, 752, 714, 603, 487 cm^{-1}; ^1H NMR (250 MHz, $CDCl_3$): $\delta = 2.23$ (dptpt, $J_d = 12.1$ Hz, $J_{1pt} = 6.1$ Hz, $J_{2pt} = 1.0$ Hz, 1H, 1′-H), 4.86 (d, $J = 12.1$ Hz, 1H, 2-H), 5.01–5.09 (m, 1H, 2′/7′-H), 5.33–5.43 (m, 1H, 2′/7′-H), 6.11–6.20 (m, 1H, 3′/6′-H), 6.39–6.48 (m, 1H, 3′/6′-H), 6.59–6.82 (m, 4H, 2 × phenyl-H, 4′-H, 5′-H), 6.97–7.05 (m, 2H, phenyl-H), 7.20–7.41 (m, 6H, phenyl-H); MS (NI-DCIMS, NH_3): *m/z*: 334 $[M]^{\bullet-}$, 244 $[M - C_7H_7]^{\bullet-}$; elemental analysis calcd (%) for $C_{24}H_{18}N_2$: C 86.20, H 5.43, N 8.38, found C 85.51, H 5.43, N 8.14.

1,8a-Dihydro-2,3-diphenylazulene-1,1-dicarbonitrile (2A): Compound **2A** was prepared in an analogous manner to the synthesis of **1A** from **8b** (1.3 g, 3.9 mmol) and $NOBF_4$ (0.91 g, 7.8 mmol) at −20 °C in the first step and pyridine (0.65 mL, 8 mmol) in the second step. The title compound was prepared as a greenish-yellow solid (0.56 g, 1.7 mmol, 44%). M.p. 104 °C; IR (KBr): $\tilde{\nu} =$ 3028, 2929, 2245, 1624, 1492, 1444, 1385, 1077, 1029, 769, 718, 698, 674 cm^{-1}; ^1H NMR (250 MHz, $CDCl_3$): $\delta = 3.71–3.76$ (m, 1H, 8a-H), 5.79–5.86 (m, 1H, 8-H), 6.05–6.10 (m, 1H, 4-H), 6.31–6.39 (m, 1H, 7-H), 6.47–6.62 (m, 2H, 5-H, 6-H), 7.13–7.40 (m, 10H, phenyl-H); MS (70 eV, EI): *m/z* (%): 332 (79) $[M]^{\bullet+}$; elemental analysis calcd (%) for $C_{24}H_{16}N_2$: C 86.72, H 4.85, N 8.43; found C 86.34, H 4.99, N 8.24.

1,2-Diphenyl-2-(2′,4′,6′-cycloheptatriene-1′-ylidene)ethylidenepropanedinitrile (2B): Compound **2B** was prepared by irradiation of solutions of **2A** in various solvents.

UV/Vis steady-state and time-resolved measurements: The molar absorption coefficient of **1A** and **2A** in acetonitrile is $\varepsilon_{342} = 1.0 \times 10^4$ and $\varepsilon_{341} = 1.0 \times 10^4\ M^{-1}cm^{-1}$, respectively. The solvents (Merck) were analytical quality, for example, DMF or Uvasol quality, for example, acetonitrile. MCH was purified by passing through a basic alumina column (Woelm); MTHF, toluene and ethanol were distilled.

Steady-state measurements were performed using absorption spectrophotometers (Perkin–Elmer 554 and HP 8453) and spectrofluorimeters (Spex-Fluorolog and Perkin–Elmer, LS-5). The Φ_f values were obtained as reported previously.[12] Continuous irradiation was carried out using a 1000 W Hg/Xe lamp combined with a monochromator or a 254 nm low pressure Hg lamp for $\lambda_{irr} = 254$ nm. The absorption increase (A^1) at low conversion as a function of t_{irr} was used to measure the quantum yields of products. The overall quantum yield of colouration of systems **1** and **2** was obtained from the increase in absorption at $\lambda_{col} = 460–510$ nm versus t_{irr}. For **1** more specifically the quantum yields $\Phi_{\mathbf{A}\rightarrow\mathbf{B}}$ and $\Phi_{\mathbf{A}\rightarrow\mathbf{C}}$ were determined from the absorption increases in the visible range (using $\lambda_{\mathbf{B}}$ and $\lambda_{\mathbf{C}}$ in Table 1) and taking the thermal relaxation into account. For each dose the A^1 value refers to the sum of Φ values and A_e to $\Phi_{\mathbf{A}\rightarrow\mathbf{C}}$. Alternatively, the absorption increase at 300–315 and 360 nm was used for $\Phi_{\mathbf{A}\rightarrow\mathbf{B}}$ and $\Phi_{\mathbf{A}\rightarrow\mathbf{C}}$, respectively. For **2** in MCH $\Phi_{\mathbf{A}\rightarrow\mathbf{B}}$ is the same using either $\lambda_{obs} = 310$ or 460 nm. The absolute Φ values were measured using the aberchrome 540 actinometry with $\varepsilon_{494} = 8.2 \times 10^3\ M^{-1}cm^{-1}$ and $\Phi = 0.20$ in toluene.[31] The pre-irradiated actinometer solution was also used to measure Φ_{-col}.

0947-6539/01/0705-1038 $ 17.50+.50/0 *Chem. Eur. J.* **2001**, *7*, No. 5

The quantum yield measurements are generally restricted by the thermal relaxation. The photoinduced value using a given t_{irr} (A^1) reverts back when the light is removed and reaches a remaining final value. The relaxation time $\tau_{\mathbf{B}\rightarrow\mathbf{A}}$ was obtained from the first-order decay or increase of $A'/A'_{max} = (A_t - A_e)/(A^1 - A_e)$ at an appropriate wavelength. When t_{irr} is short with respect to $\tau_{\mathbf{B}\rightarrow\mathbf{A}}$, the absorbance at λ_{col} increases with t_{irr}, whereas in the other cases a photostationary state is already approached at low conversion. This is in contrast to system **3**, where $\tau_{\mathbf{B}\rightarrow\mathbf{A}}$ is longer by more than three orders of magnitude.[12] At 25 °C the condition $t_{irr} < \tau_{\mathbf{B}\rightarrow\mathbf{A}}$ can be achieved for **1** and **2** even in nonpolar solvents only for low conversion using $\lambda_{irr} = 366$, 313 or 254 nm. Upon repeated irradiation at 366 nm followed by thermal relaxation of **1** and **2** in several solvents, the samples remain essentially intact. Nevertheless, they can eventually be destroyed upon prolonged irradiation. This decomposition was found to be significant for **1** in ethanol, where the absorption spectrum becomes broader and the band at 340 nm decreases. For **2** in ethanol the absorption spectrum increases below 340 nm and decreases above.

Laser flash photolysis (time resolution of 15–20 ns) was carried out using $\lambda_{exc} = 530$, 354 or 308 nm from the second and third harmonics of a neodymium laser or an excimer laser, respectively.[12, 13] In some cases $\lambda_{exc} =$ 248 nm from another excimer laser was applied. For pulsed excitation (at 308 nm) an appropriate wavelength, for example, $\lambda_{obs} = 473$ nm, was used for determining the rate constant of the relaxation kinetics. The relative yield (ΔA_{col}) was obtained from the linear part of the absorption increase at the long wavelength maximum (λ_{col}) versus the laser intensity using optically matched solutions.

Computational methods: Pre-optimisation of the molecular structures was achieved using the force-field methods implemented in Moby 1.4.[32] Semiempirical calculations were performed with the programs WinMopac 2.0[33] and Vamp 6.5[34] using the AM1- (**2A**) and PM3- (**1A,B** and **2A,B**) Hamiltonians, respectively, under the EF formalism. All optimised structures (transition states and minima) were proved to be stationary points by analysing the Hessian. Transition states (TS1, TS2) were also successfully used in intrinsic reaction co-ordinate (IRC) calculations. Additionally, the TRIPOS-force-field implemented in Sybyl 6.6 was applied to estimate the rotational barrier of the s-*trans*-VHF → s-*cis*-VHF isomerisation (TS2) of **2A**.[35] Solvent effects (system **1** and **2**) were calculated with the conductor-like screening model (COSMO)[36] provided by WinMopac 2.0. In case of system **1** the solvent was also modelled by the self-consistent reaction field method (SCRF[37], Vamp 6.5). All systems were treated without using configuration interaction (CI). Additionally, for system **1**, CI was used as implemented in Vamp, considering all singly and doubly paired excitations in the calculation with respect to ten fully occupied and ten virtual orbitals.

Acknowledgements

T.M. is a recipient of the Stipendium zur Förderung des wissenschaftlichen und künstlerischen Nachwuchses. We thank Professor Kurt Schaffner for his support, Professor S. Dove for performing the TRIPOS-force-field calculations and valuable discussion, Dr. M. Zabel for performing the X-ray structure analysis and Mr. L. J. Currell and M. Steinhäuser for technical assistance.

[1] a) *Photochromism* (Ed.: G. H. Brown) in *Techniques of Chemistry*, *Vol. III* (Ed.: A. Weissberger), Wiley, New York, **1971**; b) *Photochromism*, *Molecules and Systems Studies in Organic Chemistry 40* (Eds.: H. Dürr, H. Bouas-Laurent), Elsevier, Amsterdam, **1990**; c) J. C. Crano, R. J. Guglielmetti, *Organic Photochromic and Thermochromic Compounds*, Vol. *1 & 2*, Plenum Press, New York, **1999**; d) J. Daub, T. Mrozek, A. Ajayaghosh, *Mol. Cryst. Liq. Cryst*. **2000**, *344*, 41.

[2] B. L. Feringa, W. F. Jager, B. de Lange, *Tetrahedron* **1993**, *49*, 8267.

[3] a) V. I. Minkin, V. A. Bren′, A. E. Lynbarskaya "*Organic Photochromes for Solar Energy Storage*" in *Organic Photochromes* (Ed.: A. V. El′tsov), Consultants Bureau, New York, **1990**, Chapter 5, p. 229; b) K. Koyama, N. Yamaguchi, T. Miyasaka, *Adv. Mater.* **1995**, *7*, 590.

[4] R. R. Birge, R. B. Gross, A. F. Lawrence "*Biomolecular Electronics and Optical Computing*" in *Molecular Electronics—Properties*, *Dynamics*, *and Applications* (Eds.: G. Mahler, V. May, M. Schreiber), Marcel Dekker, Inc., New York, **1996**, Chapter 15, p. 333.

[5] a) J. C. Crano, T. Flood, D. Knowles, A. Kumar, B. Van Gemert, *Pure Appl. Chem*. **1996**, *68*, 1395; b) C. Bräuchle, N. Hampp, D. Oesterhelt, *Adv. Mater*. **1991**, *3*, 420; c) J.-M. Lehn, *Supramolecular Chemistry*, VCH, Weinheim, **1995**; d) F. Vögtle, *Supramolekulare Chemie*, Teubner, Stuttgart, **1992**, Chapter 7.

[6] a) O. Pieroni, A. Fissi, G. Popova, *Prog. Polym. Sci*. **1998**, *23*, 81; b) J. Stumpe, T. Fischer, M. Roloh, J. G. Meier, *Polym. Prep*. **1998**, *39*, 308.

[7] J. Peretti, J. Biteau, J.-P. Boilot, F. Chaput, V. I. Safarov, J.-M. Lehn, A. Fernandez-Acebes, *Appl. Phys. Lett*. **1999**, *74*, 1657.

[8] a) C. Bräuchle, N. Hampp, D. Oesterhelt "*Bacteriorhodopsin-Optical Processor Molecules from Nature*" in *Molecular Electronics*, *Properties*, *Dynamics*, *and Application* (Eds.: G. Mahler, V. May, M. Schreiber), Marcel Dekker, New York, **1996**, p. 359; b) K. Schaffner, S. E. Braslavsky, A. R. Holzwarth, *Adv. Photochem.* **1990**, *15*, 229.

[9] *Multifold* switching is used for the switching of systems with addressable subunits of the same kind and structure, which are activated by the same physical stimulus and lead to the same A/B-transformation. *Multimode* switching denotes switchable systems containing either more than one switching subunit which differ in structure or which are stimulated by different chemical or physical activation as for example in the case of redox-switchable photochromic dyes.

[10] S. Gierisch, W. Bauer, T. Burgemeister, J. Daub, *Chem. Ber.* **1989**, *122*, 2341.

[11] a) J. Daub, T. Knöchel, A. Mannschreck, *Angew. Chem.* **1984**, *96*, 980; *Angew. Chem. Int. Ed. Engl.* **1984**, *23*, 960; b) J. Daub, S. Gierisch, U. Klement, T. Knöchel, G. Maas, U. Seitz, *Chem. Ber.* **1986**, *119*, 2631; c) S. Gierisch, J. Daub, *Chem. Ber.* **1989**, *122*, 69; d) J. Daub, J. Salbeck, T. Knöchel, C. Fischer, H. Kunkely, K. M. Rapp, *Angew. Chem.* **1989**, *101*, 1541; *Angew. Chem. Int. Ed. Engl.* **1989**, *28*, 1494; e) P. A. Bross, A. Mirlach, J. Salbeck, J. Daub, *Dechema Monograph.* **1990**, *121*, 375; f) J. Daub, S. Gierisch, J. Salbeck, *Tetrahedron Lett.* **1990**, *31*, 3113; g) J. Daub, C. Fischer, F. Salbeck, K. Ulrich, *Adv. Mater.* **1990**, *2*, 366; h) J. Achatz, C. Fischer, J. Salbeck, J. Daub, *J. Chem. Soc. Chem. Commun.* **1991**, 504; i) H. Spreitzer, J. Daub, *Chem. Eur. J.* **1996**, *2*, 198; j) L. Gobbi, P. Seiler, F. Diederich, *Angew. Chem.* **1999**, *111*, 740; *Angew. Chem. Int. Ed*. **1999**, *38*, 674.

[12] H. Görner, C. Fischer, S. Gierisch, J. Daub, *J. Phys. Chem.* **1993**, *97*, 4110.

[13] H. Görner, C. Fischer, J. Daub, *J. Photochem. Photobiol. A*: *Chem.* **1995**, *85*, 217.

[14] H. Spreitzer, J. Daub, *Liebigs Ann. Chem.* **1995**, 1637.

[15] T. Mrozek, *Diplom Thesis*, University of Regensburg, **1997**.

[16] a) M. Irie, K. Sayo, *J. Phys. Chem.* **1992**, *96*, 7671; b) M. Irie, *Pure Appl. Chem.* **1996**, *68*, 1367.

[17] a) M. Irie, K. Sakemura, M. Okinaka, K. Uchida, *J. Org. Chem*. **1995**, *60*, 8305; b) M. Irie, T. Eriguchi, T. Takada, K. Uchida, *Tetrahedron* **1997**, *53*, 12263; c) M. Irie, K. Uchida, *Bull. Chem. Soc. Jpn*. **1998**, *71*, 985.

[18] G. M. Tsivgoulis, J.-M. Lehn, *Chem. Eur. J.* **1996**, *2*, 1399.

[19] A. T. Bens, D. Frewert, K. Kodatis, C. Kryschi, H.-D. Martin, H. T. Trommsdorf, *Eur. J. Org. Chem.* **1998**, 2333.

[20] T. Mrozek, H. Görner, J. Daub, *Chem. Commun.* **1999**, 1487.

[21] a) G. Gurzadyan, < 10 ps, private communication, **1999**; b) for fs-resolved UV/Vis-spectroscopic investigations on the DHA/VHF-systems, see also: c) J. Ern, M. Petermann, T. Mrozek, J. Daub, K. Kuldová, C. Kryschi, *Chem. Phys.* **2000**, *259*, 331; d) M. Beutter, E. Riedle, T. Mrozek, J. Daub, unpublished results.

[22] a) Semiempirical methods are often found to underestimate rotational barriers of butadiene systems (e.g. in vinylheptafulvenes): b) *Quantenchemie* (Ed.: H.-H. Schmidtke), 2nd ed., VCH, Weinheim, **1994**, Chapter 11.2.4; c) F. Jensen, *Introduction to Computational Chemistry*, Wiley, New York, **1999**, Chapter 3.10.5. Therefore TRIPOS-force-field calculations (Sybyl 6.6) were additionally applied to estimate the rotational barrier TS2. The respective findings support the results from the PM3 calculations (vacuum): $\Delta\Delta H_f$ of **DPE**-s-*cis*-**VHF** → TS2: 19 kJ mol^{-1}; $\Delta\Delta H_f$ of **DPE**-s-*trans*-**VHF** → TS2: 8 kJ mol^{-1}. d) Analogues results have been obtained from AM1- and PM3 calculation concerning the ring closure reaction (s-*trans*-VHF →

DHA) of different DHA/VHF derivatives (A. Knorr, *Diplomathesis*, University of Regensburg, **1992**). Similar investigations have been performed on related photochromic systems P. N. Day, Z. Wang, R. Pachter, *J. Phys. Chem*. **1995**, *99*, 9730; e) see ref. [22c], Chapter 3.11 and ref. [22b].

[23] For analogues reactions seea) K. A. Muszkat, M. Eisenstein, E. Fischer, A. Wagner, Y. Ittah, W. Lüttke, *J. Am. Chem. Soc*. **1997**, *119*, 9351; b) K. Muszkat, E. Fischer, *J. Chem. Soc. B* **1967**, 662.

[24] Note that the photochemically induced ring-opening reaction was found to proceed by an ultrafast mechanism which is believed to be due to a conical intersection between the S_1- and S_0-potential energy hypersurfaces. These findings indicate that the thermal ground state cyclisation proceeds along a completely different reaction coordinate compared with the photochemical pathway.

[25] a) J. Cosier, A. M. Glazer, *J. Appl. Crystallogr*. **1986**, *19*, 105; b) A. Altomare, G. Cascarano, C. Giacovazzo, C. Guagliardi, A. Guagliardi, *J. Appl. Crystallogr.* **1993**, *26*, 343.

[26] a) G. M. Sheldrick, *SHELXL97-Program for crystal structure refinement*, University of Göttingen, **1993**; b) M. N. Burnett, C. K. Johnson, *ORTEP-III*: *Oak Ridge Thermal Ellipsoid Plot Program for Crystal Structure Illustration*, Oak Ridge National Laboratory Report ORNL-6895, **1996**.

[27] Crystallographic data (excluding structure factors) for the structure reported in this paper have been deposited with the Cambridge Crystallographic Data Centre as supplementary publication no. CCDC-143892. Copies of the data can be obtained free of charge on application to CCDC, 12 Union Road, Cambridge CB21EZ, UK (fax: (+44) 1223-336-033; e-mail: deposit@ccdc.cam.ac.uk)..

[28] D. W. Wiley, B. C. McKusick, *Org. Synth*. **1963**, *43*, 101.

[29] J. B. Press, J. J. Nally, *J. Heterocycl. Chem*. **1988**, *22*, 1571.

[30] K. Nanjo, K. Suzuki, M. Sekiya, *Chem. Bull. Pharm*. **1977**, *25*, 2396.

[31] H. G. Heller, J. R. Langan, *J. Chem. Soc. Perkin Trans. 2* **1981**, 2341.

[32] U. Höweler, MOBY 1.4, Springer, Heidelberg, **1991**.

[33] *WinMOPAC 2.0*, Fujitsu Ltd., Computer Chemistry Systems Dept., Nakase, Japan, **1997**–**1998**.

[34] G. Rauhut, A. Alex, J. Chandrasekhar, T. Steinke, W. Sauer, B. Beck, M. Hutter, P. Gedeck, T. Clark, *VAMP 6.5*, Erlangen, **1996**.

[35] *SYBYL 6.6*, TRIPOS, St. Louis, USA, **1999**.

[36] A. Klamt, G. Schüürmann, *J. Chem. Soc. Perkin Trans. 2* **1993**, 799.

[37] G. Rauhut, T. Clark, *J. Am. Chem. Soc*. **1993**, *115*, 9174.

Received: June 13, 2000 [F2541]

0947-6539/01/0705-1040 $ 17.50+.50/0